Distribution of cluster sizes from evaporation to total multifragmentation

A. Z. Mekjian
Department of Physics and Astronomy, Rutgers University, Piscataway, New Jersey 08855
(Received 8 December 1989)

A model for studying fragmentation phenomena is proposed and developed. The model leads to a single, simple, and exact expression for the cluster size distribution function. Various limits of this distribution function show: (1) evaporation-like behavior, (2) scale-invariant power law behavior, (3) a broad region with a dependence which is linear growth in small clusters and exponential falloff of large clusters and, finally, (4) total multifragmentation with an exponential-like falloff of all clusters except the monomer or unit element. The cluster size distribution function in any region is given by various limits of one expression: $Y_A(k,x)=\{A!/[k!(A-k)!]\}xB(x+A-k,k)$. Here, the size k is the number of elements in a cluster taken from a fixed total number of A elements, x is an evolutionary tuning parameter which determines the various regions, and $B(x+A-k,k)$ is a beta function. Cellular rules and a particular choice of weight function lead to self-similar behavior on Young's triangular lattice. A scale invariant hyperbolic power law emerges in a row by row evolution of the lattice. A counterclockwise rotation of Ferrer's block diagram of partitions shows a pictorial resemblance of the present model with recent work on self-organized critical states, and a comparison is made. The cumulative mass distribution at a critical point of the model is a staircase function whose continuous limit is analogous to that of a uniform bar. The uniform bar may then be hammered into various shapes which will be discussed. Some observations on the form of x are given by comparing the multifragmentation limit of the model with the law of mass action or Saha equation. The evaporation limit of the model is discussed and evaporation barriers are shown to evolve into binding energy enhancement factors in the Saha equation.

I. INTRODUCTION

Cascading phenomena, fragmentation processes and their related inverses, clustering, and connectivity problems are of current interest in many different fields. As an example, heavy-ion collisions from low to very high energies can be used to explore nuclear fragmentation phenomena and cluster distributions. One of the primary quantities of interest is the distribution of products of such collisions in composition space which is called the cluster size distribution function. The cluster size distribution function is the mean (ensemble averaged) number of clusters of a given size plotted versus the size of various clusters. The size of a nuclear cluster is determined by the number of nucleons. An evaporation process appears in the distribution function as a large fragment plus a small fragment, usually a single nucleon. A critical point manifests itself as a power law falloff in the cluster distribution function. Total multifragmentation is here taken to mean a very high multiplicity plus a much faster falloff than a power law in the fragment distribution function. The multiplicity is the total number of fragments produced in the collision.

The cluster size distribution is of primary interest in many other studies. Some examples are the following: in percolation studies on a lattice,[1] in the size distribution of meteorites,[2] in the size of sandpile slides at the self-organized critical point,[3] and in related models of avalanches.[4] Other variables besides cluster size can be considered and, in general, the distribution of a dependent quantity versus another intrinsic quantity can be studied. Several examples of such distributions are the number of earthquakes as a function of their energy,[5] and the spectral decomposition of noise as a function of the frequency with its interesting low-frequency $1/f$ flicker behavior.

One of the remarkable features of these distribution functions is the appearance of a power law behavior. That is, the functional behavior of the distribution function is some inverse power of the cluster size, energy, frequency, etc. Power law behaviors have been seen in cluster size distributions at the percolation threshold,[1] droplet sizes at a critical point,[6] and sandpile[3] and avalanche[4] slides at a self-organized critical point. In linguistics, a power law, called Zipf's law,[7] is found in the frequency distribution of words in a book when each word is ordered according to its frequency of occurrence. In economic phenomena, another power law, called Pareto's law,[8] appears in the distribution function of income plotted versus income. In social phenomena, Lotka's law[9] is a power law relationship between the number of authors publishing n papers, as a function of n. A more complete summary can be found in Refs. 10 and 11. In many cases, the power law is an empirically observed or tabulated property of the system. One main purpose of this paper, an initial accounting of which is given in Ref. 12, is to present an exact power law which arises in mathematics, and, in particular, in combinatorial analysis and permutation groups. Then, it is shown how this mathematical result has a physical significance in fragmentation phenomena. A model of a fragmentation process is presented and developed. At a particular value of

some evolutionary tuning parameter, this power law emerges in the cluster size distribution function. The scale-invariant power law behavior is interpreted in terms of the appearance of self-similar structure produced by cellular rules on Young's triangular lattice of partitions.

Moreover, the model proposed here is exactly soluble for all values of the evolutionary tuning parameter. As the evolutionary parameter is changed, a system evolves through all its modes of fragmentation. At low values of this parameter, evaporation modes dominate, and at high values of it, multifragmentation takes place. The behavior near the scalar invariant point can also be easily analyzed, and results concerning cluster sizes near this point are presented. A cumulative mass distribution of cluster sizes is introduced and studied. This distribution is found to be a staircase function near the scale-invariant point, and its continuum limit is analogous to the mass distribution of a uniform bar. The bar is hammered into various shapes by varying the evolutionary tuning parameter. Another, more exotic way, turns the cumulative mass distribution into Cantor's devil's staircase. Finally, some observations on the form of the tuning parameter x are given by comparing the multifragmentation limit with a model developed previously[13] to describe high-energy nucleus-nucleus collisions. The fragmentation model proposed and developed in this paper may have applications for understanding similar behavior in other systems. Some discussion of its relevance to other areas is given.

II. A MODEL OF A FRAGMENTATION PROCESS

A. General remarks

The model developed below evolved from some studies of nuclear fragmentation started in Ref. 13 and continued in a series of papers.[14–17] Considerable interest exists in the problem of the fragmentation of a nucleus, and this problem is being actively pursued by many groups.[18–27] Rather than pursuing an approach of increasing complexity and detail, the approach taken below is to simplify the problem to the point where a simple and mathematically exact solution emerges. It is hoped that the exact solution to a simplified approach still contains the essence of the more detailed models.

Simplified models in other areas have been very useful for understanding the solution to the behavior of complex systems. An example of a recent approach is given in Ref. 28, where specific cellular automata rules are applied to many different problems. One of the reasons for presenting the model developed in this paper is to give a mathematically exact solution to a specific model which, hopefully, in the future may be linked to these other approaches. While these other approaches seem to be very different from that taken here, properties of the cluster size distribution are very similar indeed.

B. Mathematical framework

1. Partitions

The model to be developed considers the partitioning of A objects into groups with n_j composites or clusters of j elements. The $j=1,2,\ldots,A$ and spans all cluster sizes from the monomer or unit cluster to a cluster made of A elements. A constraint exists which is $A=\sum jn_j$, and this constraint is a statement that the fundamental units are conserved. The system considered is therefore a closed system in A. The partitioning of A objects into such groupings can be related to a well-known problem in number theory,[29] which is the decomposition of an integer A into integer summands, and an example is given in Table I. The notation $\pi_A=(1^{n_1},2^{n_2},\ldots,j^{n_j},\ldots)$ is usually used to specify a particular decomposition. Such partitioning also appears in the classification of permutations by cycle classes,[30] with a cycle class being specified by $(n_1,n_2,\ldots,n_j,\ldots)$. In the permutation case, the j specifies the length of a cycle, and the division $(n_1,n_2,\ldots,n_j,\ldots)$ has n_1 unit cycles, n_2 cycles of length 2, etc.

The partition π_A is used to classify a given fragmentation. In the nuclear case, $\pi_A=(1^{n_1},2^{n_2},\ldots,j^{n_j},\ldots)$ corresponds to a fragmentation into n_1 nucleons, n_2 clusters made of two nucleons, and so on to n_j clusters made of j nucleons. The multiplicity of a given fragmentation, partition or cycle class decomposition is

$$m=n_1+n_2+\cdots+n_j+\cdots+n_A\ .$$

Table I groups the various partitions according to m which can run from $m=1$ to $m=A$. The $m=1$ multiplicity corresponds to a giant cluster of all A elements, the $m=2$ situation consists of a division of A into two pieces, while $m=A$ corresponds to a fragmentation into all monomers or unit elements.

The total number of partitions of A is given, for large A, by the Hardy-Ramanujan result[31]

$$P(A)=\frac{e^{\pi\sqrt{2A/3}}}{4\pi\sqrt{3}A}\ . \tag{1}$$

The number of partitions of A is obtained from a generating function

$$\sum_{A=0}^{\infty}P(A)x^A=\prod_{A=1}^{\infty}(1-x^A)^{-1}\ . \tag{2}$$

The number of partitions of A with a fixed multiplicity m is $P(m,A)$. The $P(m,A)$ satisfy a recurrence relationship

$$P(m,A)=P(m-1,A-1)+P(m,A-m)\ . \tag{3}$$

Features of $P(m,A)$ in the nuclear case can be found in Ref. 19 and will not be pursued here.

2. Young's lattice, cellular generation rules, and Ferrer's diagram

A diagrammatic view of the partitions of A, known as Young's lattice,[32] is shown in Fig. 1 for $A=1,2,\ldots,7$. Each partition is represented by a box or cell. A row in Young's lattice gives all partitions of the left-most element of the row. Rows are connected in a downward direction by adding a single unit to each cell in a row. Specifically, adding a single unit to the partition cell

TABLE I. Partitions and Cauchy numbers M_2 for $A = 10$.

A	m	π	M_2	n	m	π	M_2
10	1	10	362 880	10		$2^3,4$	18 900
	2	1,9	403 200			$2^2,3^2$	25 200
		2,8	226 800		5	$1^4,6$	25 200
		3,7	172 800			$1^3,2,5$	60 480
		4,6	151 200			$1^3,3,4$	50 400
		5^2	72 576			$1^2,2^2,4$	56 700
	3	$1^2,8$	226 800			$1^2,2,3^2$	50 400
		1,2,7,	259 200			$1,2^3,3$	25 200
		1,3,6	201 600			2^5	945
		1,4,5,	181 440		6	$1^5,5$	6 048
		$2^2,6$	75 600			$1^4,2,4$	18 900
		2,3,5,	120 960			$1^4,3^2$	8 400
		$2,4^2$	56 700			$1^3,2^2,3$	25 200
		$3^2,4$	50 400			$1^2,2^4$	4 725
	4	$1^3,7$	86 400		7	$1^6,4$	1 260
		$1^2,2,6$	151 200			$1^5,2,3$	5 040
		$1^2,3,5$	120 960			$1^4,2^3$	3 150
		$1^2,4^2$	56 700		8	$1^7,3$	240
		$1,2^2,5$	90 720			$1^6,2^2$	630
		1,2,3,4	151 200		9	$1^8,2$	45
v		$1,3^3$	22 400		10	1^{10}	1

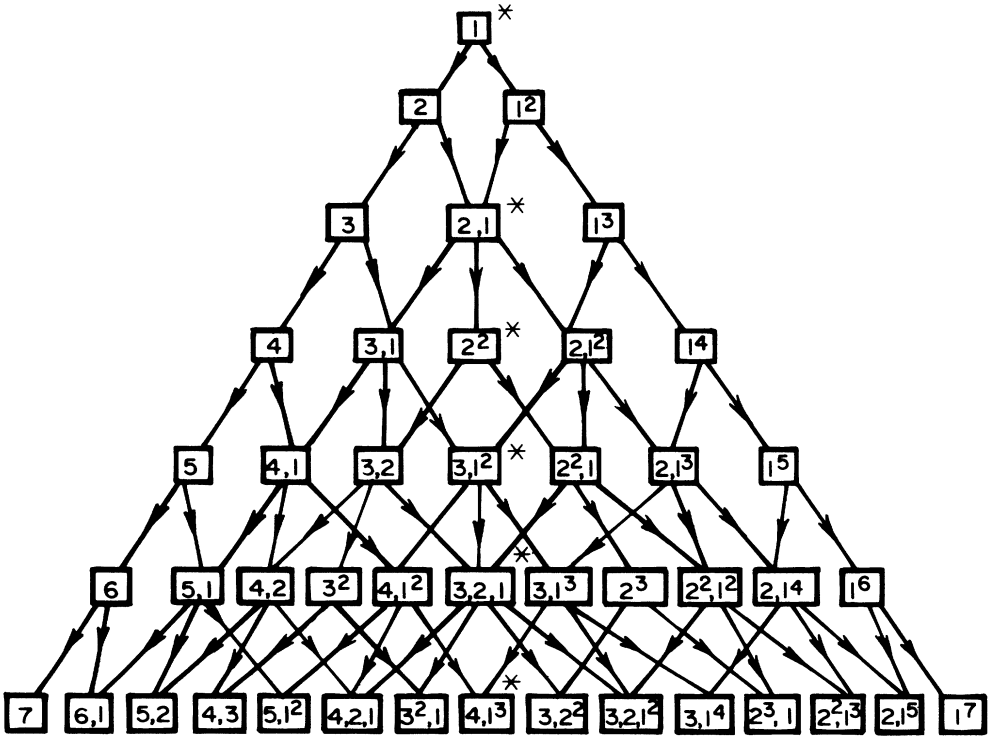

FIG. 1. Young's lattice. Young's triangular shaped lattice is used to illustrate the various partitions of A, for $A = 1-7$. Each partition of A is a cell or box of the form $[1^{n_1},2^{n_2},\ldots,A^{n_A}]$. Cellular rules can be used to generate the lattice in a row by row evolution as discussed in the text. A hidden mathematical self-similarity in this triangular lattice is discussed in Sec. II B 4. Self-similarity in cellular automata models in other problems are discussed in Ref. 28.

$[1^3,2]$ connects this partition cell to three other cells in the next row—$[1^3,3]$, $[1^2,2^2]$, and $[1^4,2]$. A general Boolean-like cellular rule is to add one to each integer j which appears in each partition box in a given row in Young's lattice to generate the next row. The cellular rules are as follows: if $j=1$,

$$[1^{n_1},2^{n_2},\ldots]\rightarrow[1^{n_1+1},2^{n_2},\ldots]$$

and

$$[1^{n_1-1},2^{n_2+1},\ldots]$$

with the second possibility ruled out if $n_1=0$; if $j=2$,

$$[1^{n_1},2^{n_2},3^{n_3},\ldots]\rightarrow[1^{n_1},2^{n_2-1},3^{n_3+1},\ldots];$$

and if $j=k$,

$$[\ldots,k^{n_k},(k+1)^{n_{k+1}},\ldots]\rightarrow[\ldots,k^{n_k-1},(k+1)^{n_{k+1}+1},\ldots].$$

A rule for the number of lines entering a box and leaving a box is as follows: The number of lines going into a box is equal to the number of different integers in the box, while the number of lines leaving a box is equal to this number plus one. Young's triangular lattice can be developed by following these cellular rules in a downward direction, row by row. This procedure was used to develop Fig. 1.

Any given decomposition $(n_1,n_2,\ldots,n_j,\ldots)\equiv(1^{n_1},2^{n_2},\ldots,j^{n_j},\ldots)$ can be put in block form using Ferrer's diagram[30] as shown in Fig. 2(a). The number of blocks in a row is the number of elements in a cluster. The number of rows with j blocks is n_j. In the traditional Ferrer's diagram the rows are arranged so that the smallest row occurs at the bottom and the largest row is at the top. Here, a rotation of Ferrer's diagram by 90° is proposed so that a row now becomes a column and the number of blocks in a column is the number of elements in a cluster. The proposed new diagram is shown in Fig. 2(b). The reason for proposing this new way of drawing a given partition becomes clear in Fig. 2(c), where a collision of two nuclei, represented as two columns, is seen as a tumbling of blocks or collapse of the initial partition. A possible final collapsed partition after a collision is also shown in Fig. 2(c). The final distribution can be produced by slides of single blocks and groups of blocks off the two columns. The total mass of a fragmentation $\sum kn_k=A_1+A_2$, the mass of the target and projectile. A weight function for the slide to the final partition is given in the next subsection. Finally, Fig. 3 illustrates a more complex fragmentation partition.

3. *Cauchy and Stirling numbers—weight functions of a soluble model*

How a given system fragments is determined by the weight function that is given to a particular partition. These weight functions are microstate counting factors. One procedure is to weight each partition according to an exponential of the entropy divided by Boltzmann's constant k for each partition. A model is then taken for the entropy functional. A possibility for the entropy in

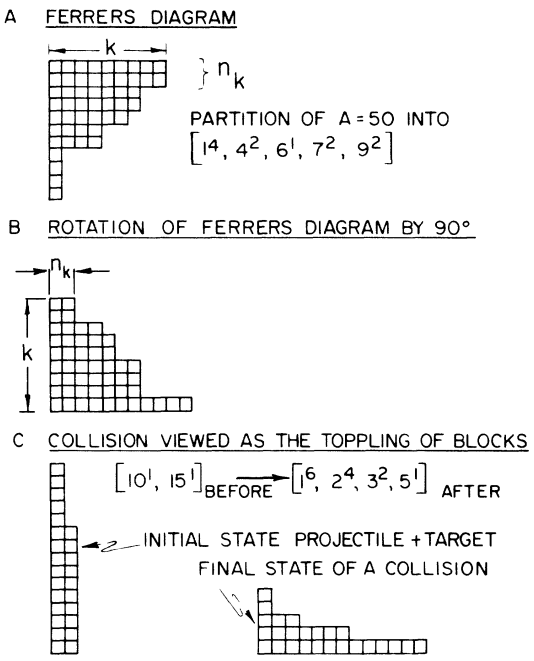

FIG. 2. Ferrer's block diagram. Ferrer's block diagram is used to represent a given partition cell of Young's lattice. Conjugate partitions are obtained by rotation of a given block diagram around a 45° diagonal. The middle elements of the first seven rows in Young's lattice are self-conjugate and have an asterisk; conjugate partitions are placed equidistant from the middle. In part (b), Ferrer's row form in k is rotated counterclockwise by 90° to change its form to a column form in k. Part (c) shows a collision of two columns of blocks, the target, and projectile partitions. A collapsed staircase partition, resulting from this collision, is produced by a toppling or sliding of blocks off the columns. A pictorial resemblance of part (c) with recent work on self-organized critical states is seen. However, the rules of the two approaches are different and the model here is closed in A. A weight for various fragmentation partitions of the present model is given in Sec. II B 3.

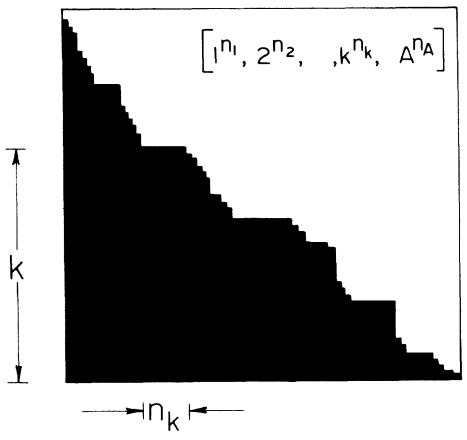

FIG. 3. A giant Ferrer's block partition in rotated form. This monstrous partition may arise from the collision of two heavy nuclei.

the nuclear case is the Sakur-Tetrode form given in Ref. 17, and generalized to include internal excitations in a cluster in Ref. 17. Maximizing the entropy subject to various constraints gives the most probable configuration which can be approximated by grand canonical ensemble results. Such approaches to nuclear multifragmentation can be found in Refs. 13–25. Another possibility is to assume each partition is equally likely.[26,27]

Here a particular form for the weight function is proposed which leads to an exactly soluble model, and the possible connection with an entropy weight will be mentioned. An un-normalized weight function of a given partition $(n_1,n_2,\ldots,n_j,\ldots)$ which gives rise to an exactly soluble model[12] is

$$\omega_A(\{n_j\},x)=M_2(\{n_j\})x^m \ . \tag{4}$$

The x is an evolutionary tuning parameter and the $M_2(\{n_j\})$ is

$$M_2(\{n_j\})=\frac{A!}{n_1!1^{n_1}n_2!2^{n_2}\cdots n_j!j^{n_j}\cdots} \ . \tag{5}$$

In number theory, the M_2 is called a Cauchy number.[29,30]

First, a model with $x=1$ is studied in upcoming subsections 4 and 5. With the evolutionary parameter equal to 1, the weight function leads to a power law behavior in the cluster size distribution function. Then, in subsection 6, the weight function, with an evolutionary parameter included, is used to develop a model of a fragmentation process. The model is still exactly soluble in all regimes of the tuning parameter. A simple expression is found which shows a system evolving through all its modes of fragmentation as this tuning parameter is changed. Before giving these results, properties of M_2 and ω_A are given.

When M_2 is summed over all partitions π_A, the result is $A!$, as first shown by Cauchy. Thus, the normalized weight function for $x=1$ is $M_2/A!$. The values of M_2 for the partition given in Table I are also listed in Table I. When M_2 is summed over a given multiplicity $m=\sum n_j$, the result is a signless Stirling number of the first kind:

$$(-1)^{A-m}S_A^m=\sum_{\pi_A(m)} M_2(\{n_j\},A) \ . \tag{6}$$

The sum in this equation is restricted to the partition of A at fixed m, $\pi_A(m)$, and also the constraint $\sum jn_j=A$ is to be satisfied.

In turn, the Stirling numbers of the first kind satisfy a recurrence relationship

$$S_A^m=S_{A-1}^{m-1}-(A-1)S_{A-1}^m \tag{7}$$

and they are generated by a factorial moment generating function

$$x(x+1)\cdots(x+A-1)=\sum_m (-1)^{A-m}S_A^m x^m \ . \tag{8}$$

An expression for $|S_A^m|$, for $m\sim\ln A$, is

$$S_A^m=(A-1)!\frac{(\gamma+\ln A)^{m-1}}{(m-1)!} \ , \tag{9}$$

where γ is Euler's number, and $\gamma=0.577\,22$, and is defined by the limit

$$\gamma=\lim_{n\to\infty}\left[1+\tfrac{1}{2}+\cdots+\frac{1}{n}-\ln n\right] \ . \tag{10}$$

Note also

$$\sum_{\pi_A} M_2=\sum_{\pi_A(m)}(-1)^{A-m}S_A^m=A! \ . \tag{11}$$

These results will be used later. Some values of S_A^m are given in Table II, which are given in a Pascal-like triangular form, similar to the form used in generating the binomial coefficients. The normalized weight function when $x\neq 1$ is

$$W_A(\{n_j\},x)=\frac{M_2(\{n_j\},A)x^m}{x(x+1)\cdots(x+A-1)} \ . \tag{12}$$

Moreover, since the sum over M_2 at fixed m generates the signless Stirling numbers of the first kind, the normalized weight function for the multiplicity distribution is

$$W_A^m(x)=\frac{(-1)^{A-m}S_A^m x^m}{x(x+1)\cdots(x+A-1)} \ . \tag{13}$$

The following features of M_2 should be stated. The largest M_2 weight is the case $n_1=1$, $n_{A-1}=1$ which is a fragmentation of A into a monomer plus the remainder, a cluster of size $A-1$. The mode of fragmentation is evaporation-like. A nucleus that is slightly excited usually evaporates a nucleon[33] so that the M_2 weight is in line with what is to be expected. The M_2 is also large for $n_A=1$, which is here called the fused mode, and is a single cluster of all A initial elements. The evaporation-like fragmentation has multiplicity $m=2$, while the fused mode has multiplicity $m=1$. At $x=0$, $W_A=0$, for all partitions except the fused mode, where $W_A(n_A=1,x=0)=1$. As x increases, the fragmentation scheme evolves from fused, to evaporation-like, to more complex modes with increasingly larger values of x. Table I lists some complex modes for $A=10$, but it should be noted that at $A=200$, the total number of fragmentation schemes is $\sim 4\times 10^{12}$, and the enumeration of the $\pi_A(m)$ is quite complex except near the end points $m\cong 1$ and $m\cong A$. At $x=1$, a scale-invariant power law emerges out of the complex fragmentation schemes as discussed in the next subsection. The x acts as an evolutionary tuning parameter and gives a weight to the multiplicity of the fragmentation. A fragmentation is a change in multiplicity.

Finally, one further observation can be made about the form of the weight function. The $n_j!$ are Gibbs factorials originally introduced into the Sakur-Tetrode law by Gibbs to resolve a paradox associated with the entropy of mixing of identical gases. Such factors also appear in the Fermi-Dirac and Bose-Einstein microstate counting factors. Specifically, the number of ways of distributing n_i fermions into g_i given levels is $g_i!/[n_i!(g_i-n_i)!]$, and the $(g_i-n_i)!$ is the number of permutations of the empty level (missing particles). In the Bose-Einstein case, the microstate counting factor is $(n_i+g_i-1)!/[(g_i-1)!n_i!]$,

TABLE II. Stirling numbers of the first kind S_A^m.

				1					
			-1		1				
		2		-3		1			
	-6		11		-6		1		
24		-50		35		-10		1	
	-120		274		-225		85		-15		1
720		-1764		1624		-735		175		-21		1
	-5040		13068		-13132		6769		-1960		322		-28		1
40320		-109584		118124		-67284		22449		-4536		546		-36		1
	-362880		1026576		-1172700		723680		-269325		63273		-9450		870		-45		1

$\longrightarrow m \longrightarrow$

where the number (g_i-1) can be considered (g_i-1) identical objects or partitions.[34] In both cases, the sum of particles (n_i) plus missing particles (g_i-n_i) or partitions (g_i-1) in the denominators equals the number g_i or (n_i+g_i-1) which appears in the numerators of these expressions. By contrast, the sum of the n_j's in M_2 is not A, but rather $A=\sum jm_j$. The M_2 counts the number of permutations of A objects into groups with n_1 of unit length, n_2 of length 2, etc. The M_2 is to be divided by the overall Gibbs factorial $A!$ for proper normalization, and this division is reminiscent of what is called correct Maxwell-Boltzmann counting in statistical mechanics. The remaining factor $1/(1^{n_1}2^{n_2}\cdots A^{n_A})$ which appears in M_2 makes the problem of fragmentation completely solvable and leads to the simple closed form expression given in the abstract. The origin of such factors may arise in the nuclear case from internal partition functions of the nuclear level density as discussed in Ref. 12. Without further justification, the result of Eq. (12) may be taken as a rule for calculating ensemble averages in a model of fragmentation phenomena. Rules appear in cellular automata models[28] and in recent work on self-organized critical states.[3,4]

4. The emergence of a scale-invariant power law and the appearance of a hidden self-similar structure in Young's triangular lattice

One of the remarkable features of the weight function discussed in the previous subsection is that it leads to a power law in the cluster size distribution function. The cluster size distribution function is obtained by ensemble averaging each n_j, $j=1,\ldots,A$ over all partitions of π_A using a weight function. For $x=1$, the normalized weight function is

$$M_2(\{n_j\},A)/A!=W_A(\{n_j\},x=1)\ . \tag{14}$$

The symbol $Y_A(k,x=1)$ is used for the mean number of clusters of size k in the fragmentation of A:

$$Y_A(k,x=1)=\sum_{\pi_A} n_k M(\{n_j\},A)/A!\ . \tag{15}$$

The $Y_A(k,x=1)$ is given by[12]

$$Y_A(k,x=1)=\frac{1}{k} \tag{16}$$

for any k with the trivial constraint $1\le k\le A$. Thus, the frequency of occurrence of a cluster of size k, or a cycle of length k, or an integer k in the partitions of A, is given by a hyperbolic power law behavior in its size. The frequency of occurrence of a monomer is 1, a dimer is $\frac{1}{2}$, a k-mer is $1/k$, etc.

The power law behavior of Eq. (16) is scale invariant since no reference to A appears in the $1/k$ factor except for the trivial constraint $k\le A$. Thus, as long as k is less than any A, the frequency of occurrence of k is given by the hyperbolic expression $1/k$ and is independent of the initial A. Each subcluster in the fragmentation of A produces smaller clusters with a frequency of occurrence $1/k$. Returning to Fig. 1, each row in Young's lattice leads to a fragmentation at the point $x=1$ with a distribution having the same scale-invariant power law behavior. Every row produces a similar spectrum of fragments. This feature will be referred to as self-similarity of the model at $x=1$. The self-similarity is a characteristic feature of systems with no length scale.[11] Figure 4 illustrates some of the statements just made.

Thus, the following observation can be made. Following the cellular rules stated in subsection 2 to generate rows in Young's lattice and the weight function associated with Cauchy's number for each cell, a self-similar behavior in every row in the triangular lattice is generated. The self-similar structure is seen in the frequency of occurrence of the integers k in the partition of A into integer summands or its equivalent interpretation in terms of clusters of size k or cycles of length k. Row by row, the law $Y_A(k)=1/k$, for $k=1,2,\ldots,A$, evolves as A increases from 1 to 2 to 3, etc., and the end point $k=A$ on the hyperbola is moved one step over when

$A \rightarrow A+1$.

This subsection is concluded with the following observations. The cluster size distribution function satisfies the constraint

$$\sum_{k=1}^{A} kY_A(k,x=1)=A \ , \tag{17}$$

and its second moment is

$$\sum_{k=1}^{A} k^2 Y_A(k,x=1)=\frac{A(A+1)}{2} \ . \tag{18}$$

The zeroth moment of this hyperbolic power law is

$$\sum_{k=1}^{A} Y_A(k,x=1)=\sum_{k=1}^{A} 1/k \sim \gamma+\ln A \tag{19}$$

for large A; the third moment is

$$\sum_{k=1}^{A} k^3 Y_A(k,x=1)=\sum_{k=1}^{A} k^2=\frac{A(A+1)(2A+1)}{6} \ . \tag{20}$$

The mean multiplicity m at $x=1$ is

$$\langle m(x=1)\rangle=\left[\sum_{m=1}^{A} m(-1)^{A-m}S_A^m\right]\Big/ A!=\gamma+\ln A \tag{21}$$

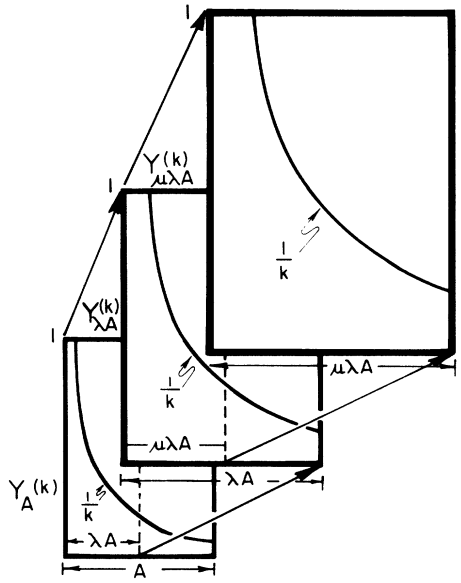

FIG. 4. Self-similarity in the cluster size distribution function. A scale invariant hyperbolic power law, $Y_A(k,x=1)=1/k$, for the fragmentation of A, is also the fragmentation law for a subcluster λA of A [$Y_{\lambda A}(k',x=1)=1/k'$] or a subcluster of λA, labeled $\mu\lambda A$ [$Y_{\mu\lambda A}(k'',x=1)=1/k''$]. The first horizontal axis is $k=1$ to A. The second horizontal axis λA gives the range of fragment sizes of λA which, in turn, is $k=1$ to λA. The third horizontal axis $\mu\lambda A$ is again, in turn, the range of fragment sizes of $\mu\lambda A$ which is $k=1$ to $\mu\lambda A$, and so on. Each subcluster taken by itself has a fragmentation scheme which is a reduced version in k of a larger cluster. At $x=1$, Young's triangular lattice of Fig. 1 has a self-similarity property in its distribution of cluster sizes.

and is just the zeroth moment of the cluster size distribution function.

5. *Staircase and uniform bar behavior of the model; hammering a solution into a devil's staircase with Cantor's rule*

The cumulative mass

$$m_k=\sum_{j=1}^{[k]+1} jY_A(j,x=1) \tag{22}$$

at $x=1$ is the staircase function shown in Fig. 5. The $[k]$ is the greatest integer in k which is taken to be continuous. This cumulative mass distribution is analogous to that of a uniform bar in the continuous limit. Adding one more unit to A shifts the point (A, A) to a new point $(A+1, A+1)$, thereby adding an extra step because the system is closed in A. In the one-dimensional sandpile slide model of Per Bak,[3] the minimally stable state (in different variables) is also a staircase function, but adding a block results in the block tumbling down the staircase and off the table when the system is open. A height difference or rise between successive steps can be defined by $\Delta_k=m_{k+1}-m_k$, which is the total mass in clusters of size $k+1$. The staircase function of Fig. 5 has $\Delta_k=1$.

Figure 5 also shows a more complex cumulative mass distribution. This staircase for a continuous bar would be Cantor's devil's staircase and would have a mass distribution which is fractally homogeneous.[11] Such a distribu-

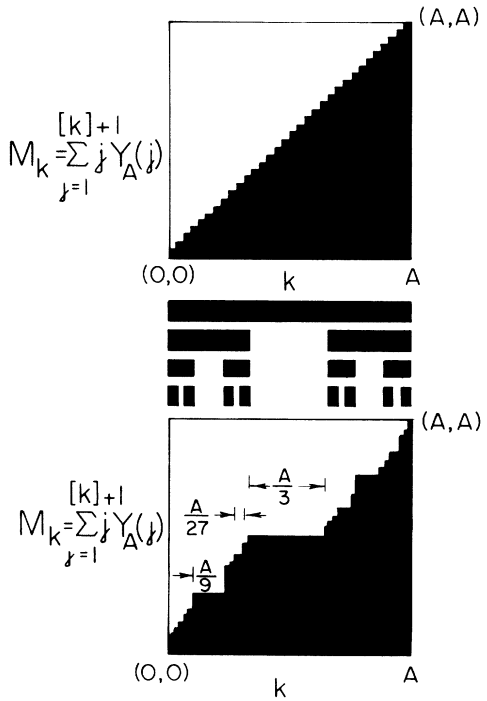

FIG. 5. Staircase cumulative mass distributions. The cumulative mass distribution of the critical state is a staircase function in the model developed here. The analog of this distribution is a uniform bar in the continuous limit as shown also. This figure also shows how the distribution may be hammered into Cantor's devil's staircase by another rule.

tion is produced by a different rule than the Cauchy one given here. This uniform mass bar is hammered so that all of the middle third goes into each outer third uniformly. Then the middle third of each outer third is hammered into their respective outer thirds, and so on at infinitum. The cumulative mass distribution then has long flat regions of no mass accumulation over most of its length followed by highly clustered jumps at infinitely many, infinitely small regions.[11] The lower part of Fig. 5 is drawn to reflect the discrete nature of j in Eq. (22). The distribution shown in the lower part of this figure is more of a mathematical curiosity than a situation that is physically realized, and the mathematical features of a Cantor-like model of fragmentation will be presented elsewhere. However, an outcome of the present discussion is the suggestion that the cumulative mass distribution defined by Eq. (22) be studied experimentally and theoretically for their staircase features. Other, more homogeneous and nonfractal ways to hammer the uniform bar are obtained by varying x, the evolutionary tuning parameter (see Sec. II C 9). The results on the cluster size distribution function for all values of x will now be presented

6. *An exact result for the cluster size distribution function in all regimes of x*

The model of a fragmentation process proposed in the preceding subsection 3 is exactly soluble in all regimes of the tuning parameter x. The cluster size distribution function is given by

$$Y_A(k,x)=\sum_{\Pi_A} n_k W_A(\{n_j\},x) . \tag{23}$$

Using

$$W_A(\{n_j\},x)=\frac{M_2(\{n_j\},A)x^m}{x(x+1)\cdots(x+A-1)} , \tag{24}$$

the $Y_A(k,x)$ is found to be given by[12]

$$Y_A(k,x)=\frac{A!}{k(A-k)!}\frac{x\Gamma(x+A-k)}{\Gamma(x+A)} . \tag{25}$$

The gamma functions are given by $\Gamma(z)=(z-1)!$. At $x=1$, $Y_A(k,x=1)=1/k$, and the scale-invariant power law result of the preceding subsection emerges. Other limiting cases of $Y_A(k,x)$ will be given in Sec. II C.

The result of Eq. (25) can be written in various forms. The form of Eq. (25) explicitly shows the power law behavior. The coefficient $A!/(A-k)!$ is part of a binomial coefficient. Multiplying numerator and denominator of Eq. (25) by $\Gamma(k)=(k-1)!$ gives rise to a form involving a beta function $B(x+A-k,k)$ and a binomial coefficient

$$Y_A(k,x)=\frac{A!}{k!(A-k)!}[xB(x+A-k,k)] , \tag{26}$$

where

$$B(z,\omega)=\Gamma(z)\Gamma(\omega)/\Gamma(z+\omega) .$$

Other useful forms to be used later are

$$Y_A(k,x)=\frac{A!}{k(A-k)!}x\frac{x(x+1)\cdots(x+A-k-1)}{x(x+1)\cdots(x+A-1)} \tag{27}$$

and

$$Y_A(k,x)=\frac{A!}{k(A-k)!}x\frac{\sum_{n=1}^{A-k}(-1)^{A-k+n}S_{A-k}^{n}x^n}{x(x+1)\cdots(x+A-1)} . \tag{28}$$

The last form will be very useful when the contributions from various multiplicity modes m to $Y_A(k,x)$ are studied.

An approximate form for $Y_A(k,x)$ can be obtained by using Stirling's approximation for factorials, $n!\simeq n^n e^{-n}\sqrt{2\pi n}$. With some rearrangement of terms, the cluster distribution function reduces to the form

$$Y_A(k,x)\simeq\frac{\sqrt{2\pi k}\,e^{-k}}{k}(1-p)^{x+(1/2)} \times\left[\frac{A!}{k!(A-k)!}(1-p)^{A-k}p^k\right] . \tag{29}$$

The

$$p=p_A(k,x)=k/(x+A-1)$$

depends on k, x, and A. The term in square brackets has a random walk-like structure.

The next subsection studies various limiting cases of the cluster size distribution function as x is varied from 0 to 1 to ∞. Also fluctuations away from the mean number of clusters are easily obtained from the weight function, and the results will be given in Sec. II C 7.

C. Properties of the cluster size distribution function

As the evolutionary tuning parameter x is varied from 0 to ∞, the fragmentation mode varies from the fused ($x=0$) mode which has multiplicity $m=1$, through evaporation-like $m=2$ modes, to more complex $m=3$, 4, 5, etc. modes, to a scale-invariant behavior at $x=1$ and finally, as $x\to\infty$, to total multifragmentation with a multiplicity $m\to A$. This subsection presents properties of the cluster distribution function for various values of x. The division between different regions of m as x is varied is determined by the signless Stirling numbers $(-1)^{A-m}S_A^m$ and x^m since the weight function for the multiplicity distribution is

$$(-1)^{A-m}S_A^m x^m/[x(x+1)\cdots(x+A-1)] .$$

At $x=0$, $m=1$ and at $x=1$, $\langle m\rangle=\gamma+\ln A$. If the interval in x from 0 to 1 is divided into equal regions of length $1/(\gamma+\ln A)$, then new modes in m arise in each of these intervals. A more detailed evaluation of the behavior of the multiplicity distribution will be given below in Sec. II C 6.

1. *Evaporation-like region, $0\le x\le 1/(\gamma+\ln A)$*

As already noted, at $x=0$, the only cluster present is the cluster with all elements, $Y_A(A,x=0)=1$. For small

x, x in the interval $[0,1/(\gamma+\ln A)]$, the $m=2$ evaporation-like modes contribute to $Y_A(k,x)$. The cluster size distribution function for small x is obtained from the results of Sec. II B 6. The $Y_A(A,x)$ is

$$Y_A(A,x)\sim 1/A^x , \tag{30}$$

while the $Y_A(k,x)$, for $k\neq A$, is

$$Y_A(k,x)\simeq \frac{Ax}{k(A-k)} . \tag{31}$$

The last equation follows from $|S^{(1)}_{A-k}|=(A-k-1)!$ and using Eq. (28) to obtain $Y_A(k,x)$. The $Y_A(k,x)$ is a U-shaped function of x as k varies from 1 to $A-1$, and is symmetric around $A/2$. The frequency of occurrence of the largest cluster is reduced from unity and is decreasing rapidly with x. At $x=1$, $Y_A(A,x=1)=1/A$. The expression that gives $Y_A(A,x)$ exactly for all x is

$$Y_A(A,x)=\frac{A!}{A}\frac{\Gamma(x+1)}{\Gamma(x+A)} . \tag{32}$$

Use has been made of the property $x\Gamma(x)=\Gamma(x+1)$ to obtain this last result. It should be observed that at $x=0$, $\Gamma(x+1)=0!=1$ and at $x=1$, $\Gamma(x+1)=1!=1$ also. The numerator in Eq. (32) is nearly constant in the interval $x=0$ to 1.

2. *The appearance of a logarithmic asymmetry in $Y_A(k,x)$ from multiplicity $m=3$ fragmentation modes and higher modes*

In the next interval in x, x in the range $1/(\gamma+\ln A)\leq x\leq 2/(\gamma+\ln A)$, the $m=3$ modes contribute to $Y_A(k,x)$. The $m=3$ decay scheme is already quite complex, as can be seen from Table II. The $Y_A(k,x)$ is reduced further, $Y_A(k,x)=1/A^x$, since x is now larger than in the first interval. The Stirling numbers in Eq. (28) can be approximated by

$$S^n_{A-k}=(A-k-1)!\frac{(\gamma+\ln A)^{n-1}}{(n-1)!} \tag{33}$$

to evaluate $Y_A(k,x)$. The $m=2$ mode has $n=1$ because of the extra power of x in the numerator. To order x^2 in the numerator of Eq. (28), the $Y_A(k,x)$ is

$$Y_A(k,x)\cong\frac{Ax}{k(A-k)}+\frac{Ax^2\ln(A-k)}{k(A-k)} . \tag{34}$$

Small γx^2 terms have been neglected. The important feature of this $Y_A(k,x)$ is the appearance of an asymmetric contribution in k which is $A\ln(A-k)/[k(A-k)]$; for $k=1$, the asymmetric factor is $A\ln(A-1)/[1\cdot(A-1)]$, while for $k=A-1$, it is $A\ln 1/[(A-1)\cdot 1]=0$. The small k cluster distribution is larger than the $k\sim A$ part. This asymmetry is obvious at $x=1$, where $Y_A(k,x)=1/k$, $Y_A(1,1)=1$, and $Y_A(A,1)=1/A$. The $m=2$ modes give rise to a symmetric cluster distribution in k, but the $m=3$, and successive $m=4$, 5, 6, etc. modes produce a pronounced asymmetry. In fact, the contribution of higher multiplicity modes to $Y_A(k,x)$ can be summed to give the following approximate form:

$$Y_A(k,x)=\frac{Ax}{k(A-k)^{1-x}A^x}=\frac{x}{k(1-k/A)^{1-x}} \tag{35}$$

for x in the interval [0,1] and $k\neq A$.

3. *Behavior around $x=1$ and the appearance of a connnectivity function*

Properties of the cluster size distribution around $x=1$ can be obtained by substituting $x=1+\epsilon$ into Eq. (28). When $x=1+\epsilon$ is substituted into Eq. (28), the following expression is obtained:

$$Y_A(k,\epsilon)=\frac{1}{k}\left\{\frac{1+\sum_{n=1}\epsilon^n[B_n(A-k)+B_{n-1}(A-k)]}{1+\sum_{n=1}\epsilon^n B_n(A)}\right\} . \tag{36}$$

The $B_n(A)$ and $B_n(A-k)$ are binomial moments of the multiplicity distribution for A and $A-k$ evaluated at $x=1$. This multiplicity distribution is determined by the Stirling numbers $(-1)^{A-m}S^m_A/A!$. Specifically

$$B_n(A)=\sum_m\frac{m!}{(m-n)!n!}(-1)^{A-m}\frac{S^m_A}{A!} , \tag{37}$$

and similarly,

$$B_n(A-k)=\sum_m\frac{m!}{(m-n)!n!}(-1)^{A-k-m}\frac{S^m_{A-k}}{(A-k)!} . \tag{38}$$

The binomial numbers can be shown to satisfy a recurrence relationship:

$$B_n(A)=B_n(A-1)+A^{-1}B_{n-1}(A-1) . \tag{39}$$

The multiplicity distribution will be investigated in more detail in the upcoming Secs. II C 6 and II C 7. When $x=1+\epsilon$ is substituted into Eq. (25), the

$$\begin{aligned}\Gamma(1+\epsilon+A-k)&=\Gamma(1-A-k)+\epsilon\Gamma'(1+A-k)\\&=\Gamma(1+A-k)[1+\epsilon\psi(1+A-k)] ,\end{aligned} \tag{40}$$

to order ϵ in a Taylor expansion. The $\psi(z)=\Gamma'(z)/\Gamma(z)$ is a psi function or digamma function. A similar result is obtained for

$$\Gamma(1+\epsilon+A)=\Gamma(1+A)[1+\epsilon\psi(A)] . \tag{41}$$

At integer values

$$\psi(p)=-\gamma+\sum_{n=1}^{p-1}\frac{1}{n} . \tag{42}$$

To order ϵ,

$$Y_A(k,\epsilon)=\frac{1}{k}[1+\epsilon(1-C_A^k)]\ , \tag{43}$$

where the connectivity function C_A^k is

$$C_A^k=\left[1+\frac{1}{2}+\cdots+\frac{1}{A}\right]-\left[1+\frac{1}{2}+\cdots+\frac{1}{A-k}\right]\times(1-\delta_{k,A})\ . \tag{44}$$

The $\delta_{k,A}$ is 0 for $k\neq A$ and is 1 for $k=A$. The connectivity function is smallest for $k=1$, where the two sums essentially cancel, $C_A^1=1/A$; for $k=2$, $C_A^2=(1/A)+1/(A-1)\sim 2/A$ and for $k\ll A$, $C_A^k\sim k/A$. On the other hand, at $k=A$,

$$C_A^A=1+\tfrac{1}{2}+\cdots+\frac{1}{A}=\gamma+\ln A \tag{45}$$

and C_A^A is large; similarly

$$C_A^{A-1}=\tfrac{1}{2}+\tfrac{1}{3}+\cdots+\frac{1}{A}\ , \tag{46}$$

$$C_A^{A-2}=\tfrac{1}{3}+\tfrac{1}{4}+\cdots+\frac{1}{A}\ . \tag{47}$$

The C_A^k is plotted in Fig. 6(a). The physical significance of C_A^k is that a small cluster is easy to form, requiring less connections, while a large cluster is harder to make, requiring more connections. This result is reminiscent of paths on a Bethe lattice or Cayley tree.[1] The connectivity

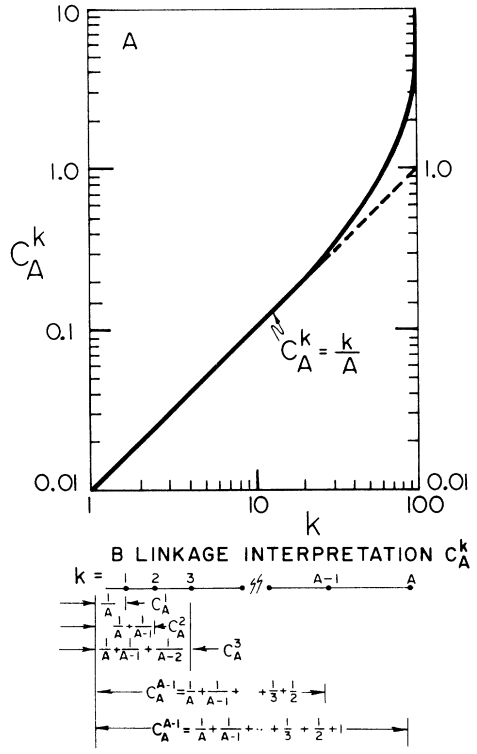

FIG. 6. The connectivity function C_A^k and a linkage interpretation of C_A^k. A break in the linear behavior of C_A^k occurs when k becomes comparable to A.

aspect or linkage nature of C_A^k is illustrated in Fig. 6(b). Each term, $1/A, 1/(A-1), \ldots, \frac{1}{2}, 1$ in C_A^k can be associated with a link of size $1/A, 1/(A-1), \ldots, \frac{1}{2}, 1$, respectively. The connectivity function C_A^k satisfies the sum rule

$$\sum_{k=1}^{A} C_A^k = A\ . \tag{48}$$

The result of Eq. (48) can be obtained by noting that there are A terms in the sum with a contribution or link size $1/A$, $A-1$ terms with a contribution or link size $1/(A-1), \ldots, 2$ terms with a contribution or link size $\frac{1}{2}, 1$ term with a contribution or link size 1. It is important to realize that as k increases both the number of links and the link size increase. But, for $k\ll A$, only the number of links contributes since the link size is $\sim 1/A$ for large A. The sum rule on C_A^k guarantees that

$$\sum_{k=1}^{A} Y_A(k,\epsilon)k = A$$

since

$$\sum_{k=1}^{A}[1+\epsilon(1-C_A^k)]=A+\epsilon A-\epsilon A=A\ .$$

The result of Eq. (43) is exact to order ϵ. For $k\ll A$, $C_A^k\sim k/A$ and

$$Y_A(k,\epsilon)=\frac{1}{k}\left[1+\epsilon\left[1-\frac{k}{A}\right]\right]\simeq\frac{1+\epsilon}{k}\left[1-\epsilon\frac{k}{A}\right]\simeq\frac{1+\epsilon}{k}e^{-\epsilon k/A}\ ; \tag{49}$$

thus

$$Y_A(k\ll A,\epsilon\ll 1)=\frac{1+\epsilon}{k}e^{-\epsilon k/A}\ . \tag{50}$$

The $Y_A(k,\epsilon)$ is no longer scale invariant if $\epsilon\neq 0$.

4. *Regions of linear growth to exponential falloff*

Above $x=1$, properties of the cluster size distribution function are easily evaluated using the gamma function or factorial representation of $Y_A(k,x)$. At integer values of x, $x=n$, the evaluation of the gamma functions are straightforward. For $x\ll A$, the large clusters decrease quickly with n:

$$Y_A(A,n)=\frac{n!}{A(A+1)\cdots(n+A-1)}\cong\frac{n!}{A^n}\ . \tag{51}$$

Then, using Stirling's approximation $n!\simeq n^n e^{-n}\sqrt{2\pi n}$,

$$Y_A(A,n)\cong\sqrt{2\pi n}\,e^{-n(\ln A-\ln n+1)}\ . \tag{52}$$

Similarly,

$$Y_A(A-1,n)=\frac{A}{A-1}n\frac{n!}{A(A+1)\cdots(n+A-1)}=\frac{A}{A-1}nY_A(A,n)\ , \tag{53}$$

$$Y_A(A-2,n)=\frac{A}{A-2}\frac{1}{2!}n(n+1)Y_A(A,n)\ , \tag{54}$$

and in general

$$Y_A(A-m,n)=\frac{A}{A-m}\frac{n(n+1)\cdots(n+m-1)}{m!}Y_A(A,n)\ . \tag{55}$$

The result of Eq. (52) is essentially an exponential decrease with n. By contrast, the small clusters increase with n. For $k=1$,

$$Y_A(1,n)=\frac{A!}{(A-1)!}n\frac{\Gamma(n+A-1)}{\Gamma(n+A)}\ , \tag{56}$$

which reduces to

$$Y_A(1,n)=n\frac{A}{n+A-1}\ . \tag{57}$$

The $Y_A(1,n)$ thus increases linearly with n, for $n\ll A$. For $k=2$,

$$Y_A(2,n)=\frac{n}{2}\frac{A(A+1)}{(n+A-1)(n+A-2)}\ , \tag{58}$$

and for $k=3$,

$$Y_A(3,n)=\frac{n}{3}\frac{A(A+1)(A+2)}{(n+A-1)(n+A-2)(n+A-3)}\ . \tag{59}$$

In general,

$$Y_A(k,n)=\frac{n}{k}\frac{A(A+1)\cdots(A+k-1)}{(n+A-1)(n+A-2)\cdots(n+A-k)}\ . \tag{60}$$

The small clusters thus grow linearly with $n=x$ for $x\ll A$. The $k=2$ cluster reaches a maximum at $x\approx A$ and $Y_A(2,x=A)\simeq A/8$. The $k=3$ cluster reaches a maximum at $x\approx A/2$ and $Y_A(3,x=A/2)\simeq 4A/81$. In general the small clusters, $k=m\ll A$, reaches a maximum at $x\approx A/(m-1)$ and

$$Y_A\left[k=m,x=\frac{A}{m-1}\right]=\frac{A}{m(m-1)}\left[1+\frac{1}{m-1}\right]^{-m}\ . \tag{61}$$

Thus, the model predicts linear growth of small clusters with x and exponential falloff with x of large clusters. The small clusters grow at the expense of large clusters. For $A=200$, the maximum values are $Y_A(2,x=A)=25$, $Y_A(3,x=A/2)\simeq 10$, $Y_A(4,x=A/3)\simeq 5$, $Y_A(5,x=A/4)\simeq 3$.

5. *Region of total multifragmentation*

When $x\gg A$, the dominant cluster is the monomer. The cluster size distribution function is

$$Y_A(k,x\gg A)\sim\frac{A!}{(A-k)!}\frac{1}{k}\frac{1}{x^{k-1}}\sim\frac{A}{k}\left[\frac{A}{x}\right]^{k-1}\ . \tag{62}$$

For $k=1$, $Y_A(1,x\to\infty)\to A$. The above equation can be rewritten as

$$Y_A(k,x\gg A)\sim\frac{A}{k}e^{-(k-1)\ln(x/A)}\ , \tag{63}$$

which is an exponential falloff with k for all k except $k=1$. Taking the ln of both sides of Eq. (63) leads to the following result:

$$\ln Y_A(k,x\gg A)=(k-1)\ln\frac{A}{x}+\ln\frac{A}{k}\ . \tag{64}$$

6. *Multiplicity distributions*

The multiplicity distribution is easily obtained from its weight function

$$W_A^m(x)=(-1)^{A-m}S_A^m x^m/[x(x+1)\cdots(x+A-1)]\ . \tag{65}$$

The mean multiplicity $\langle m\rangle=\sum mW_A^m(x)$, and is evaluated by noting $mx^m=x(\partial/\partial x)x^m$. Thus

$$\langle m\rangle=\frac{x(\partial/\partial x)D_A(x)}{D_A(x)}=1+\frac{x}{x+1}+\frac{x}{x+2}+\cdots+\frac{x}{x+A-1}\ . \tag{66}$$

Here

$$D_A(x)=x(x+1)\cdots(x+A-1)\ .$$

At $x=0$, $\langle m\rangle=1$ since only one cluster of A elements is present; at $x=1$,

$$\langle m\rangle=1+\tfrac{1}{2}+\cdots+1/A=\gamma+\ln A\ ,$$

and at $x\to\infty$, $\langle m\rangle\to A$ since the fragmentation mode approaches individual units or monomers. For $A=200$, $\langle m\rangle=5.88$ and for $A=10^{23}$, $\langle m\rangle=53$ at $x=1$. How rapidly the mean multiplicity changes with x is determined by

$$\frac{d}{dx}\langle m\rangle=\frac{1}{(x+1)^2}+\frac{2}{(x+2)^2}+\cdots+\frac{A-1}{(x+A-1)^2}\ . \tag{67}$$

The rate of change of $\langle m\rangle$ decreases uniformly with x. Consequently, unit changes in m, $\Delta m=1$, are stretched out in x with increasing x since $d\langle m\rangle/dx\sim 1/\Delta x$, where Δx is the interval size for producing a $\Delta m=1$. Also, the change in m, Δm, per unit change in x, $\Delta x=1$, is decreasing with x since $d\langle m\rangle/dx\sim\Delta m/1$ is decreasing as already noted. In the interval from 0 to 1 in x, $\Delta m=\gamma+\ln A$, and the spacing in x for unit changes in m is approximately

$$\Delta x \sim 1/(\gamma + \ln A) \sim 1/\ln A \ .$$

If this spacing were maintained from $x=0$ to $x=A$, the multiplicity at $x=A$ would be $A \ln A$, which already exceeds the limiting value $m \to A$. Again, the appearance of new modes of fragmentation requires larger changes in x as x increases.

7. Fluctuations in the model

Fluctuations in various quantities can be obtained from their respective weight functions. For example, multiplicity functions can be obtained from $W_A^m(x)$. The mean square multiplicity fluctuation is $\langle m^2 \rangle - \langle m \rangle^2$ and is simply

$$\langle m^2 \rangle - \langle m \rangle^2 = x \frac{d}{dx} m(x) = x \left[\frac{1}{(x+1)^2} + \frac{2}{(x+2)^2} + \cdots + \frac{A-1}{(x+A-1)^2} \right] , \tag{68}$$

where $m(x) = \langle m \rangle$ is given in Eq. (66). At $x=0$ and $x=\infty$, fluctuations in m vanish. At $x=1$, the fluctuations are large and of the order of $\langle m \rangle \sim \ln A + \gamma$.

8. Cluster recombinations, growth, and coagulation

The domain of x is from 0 to ∞. At $x=0$, the only cluster present is the fused mode and at $x=\infty$, monomers only exist. A simple transformation can be made to interchange the $x=0$ and $x=\infty$ point. A specific choice for such a mapping is

$$x = t_c/t \ , \tag{69}$$

which will put the fused mode at $t=\infty$, the $x=1$ point at $t=t_c$, and the monomer point at $t=0$. The behavior of $Y_A(k,t) = Y_A(k, x=t_c/t)$, with t varying from 0 to ∞, then shows a system evolving from single units to increasingly more complex cluster configurations. With increasing t, the smaller units go into making bigger clusters, and clusters combine with other clusters and monomers to make even bigger clusters. Since M_2 favors evaporation-like modes, this reverse process favors single-unit pickup by clusters. However, a weight is given to all cluster-cluster recombinations. At some point ($t=t_c$) in the evolution to a fused mode, a scale-invariant behavior emerges from the chaotic complexity of recombination processes. In t space, the cluster size distribution function is

$$Y_A(k,t) = \frac{A!}{k(A-k)!} \frac{t_c}{t} \frac{\Gamma[A-k+(t_c/t)]}{\Gamma[A+(t_c/t)]} \ , \tag{70}$$

and the multiplicity is

$$\langle m \rangle = 1 + \frac{t_c}{t_c+t} + \frac{t_c}{t_c+2t} + \cdots + \frac{t_c}{t_c+(A-1)t} \ . \tag{71}$$

Some specific properties of $Y_A(k,t)$ for the mapping of Eq. (69) are

$$Y_A(A, t > t_c) = \frac{1}{A^{t_c/t}} \ , \tag{72}$$

$$Y_A(1,t) = \frac{At_c}{At + (t_c - t)} \ . \tag{73}$$

The rate of growth of A with t, $dY_A(A,t)/dt$, is

$$\frac{dY_A(A, t > t_c)}{dt} = \frac{t_c}{t^2} \frac{1}{A^{t_c/t}} \ln A \ , \tag{74}$$

and, in reduced t and near the self-similar point $t_c/t = 1$, this rate is

$$\frac{dY_A(A, t > t_c)}{d(t/t_c)} = \frac{\ln A}{A} \ . \tag{75}$$

Other mappings such as $x = (t_c/t)^\alpha$ only change this last result by a multiplicative factor α, but have a more pronounced effect away from $t = t_c$. This last point will be discussed elsewhere, as well as mappings onto a percolation framework. Percolation studies of nuclear multifragmentation have been studied in Refs. 35, 36, 37, and 38.

9. The cumulative mass distribution in different regions of x

The cumulative mass distribution of Eq. (22) can be obtained in different regions of x from the results of Eq. (25). As already noted in Sec. II B 5, the $x=1$ solution for the cumulative mass distribution is a uniform staircase function. Each rise of each step in Fig. 5 is the same. Varying x will change the rise of each step, but the end point of the staircase is still at (A, A). Changing x also hammers the uniform bar of Fig. 5 into various homogeneous forms. Some obvious limits for the cumulative mass distribution are at $x=0$ and $x \to \infty$. The $x=0$ solution is a fused mode, and all the rise occurs in a giant last step as shown in Fig. 7(a). The mass in the bar is hammered so that all the mass is squeezed into the right end. The $x \to \infty$ limit corresponds to all the mass in monomers or single units, and the cumulative mass distribution has all the rise at the beginning as shown in Fig. 7(b). The bar is hammered so that all the mass is now squeezed on the left end.

The evaporation-like region of Sec. II C 1 has a distribution shown in Fig. 7(c), where the last step is a signal from the remaining fused mode. Figure 7(d) is the result for the cumulative mass distribution at $x \sim 2$, which corresponds to the region of linear growth of small clusters and exponential falloff of large clusters. For the case of Fig. 7(c), the bar is hammered so that more of the mass is right of the middle; for Fig. 7(d), the bar is hammered so that more of the mass is left of the middle.

D. Multifragmentation limit and the Saha equation; evaporation

In Sec. II B of this paper a model for studying fragmentation processes was proposed, and in Sec. II C solutions to the model were studied in terms of a tuning parameter

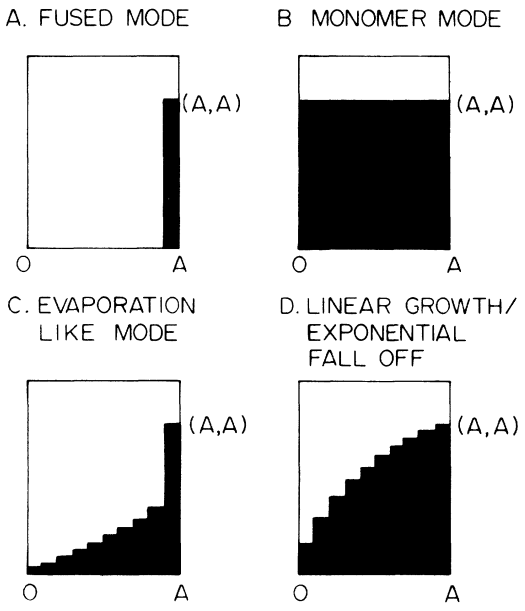

FIG. 7. The cumulative mass distribution. The cumulative mass distribution is given for different regions of x. The regions considered are as follows: part A, the $x=0$ fused mode; part B, the $x=\infty$ all monomer mode; part C, the evaporation-like mode; and part D, the region of linear growth of small clusters and exponential falloff of large clusters.

x. In this subsection a specific application of the model is studied. Specifically, the solution in the multifragmentation region given in Sec. III C 5 is compared with a previous model developed in Ref. 13. The model of Ref. 13 was used to study composite particle (cluster) formation in relativistic heavy-ion collisions. Properties of the tuning parameter x are obtained for this specific application.

The model of Ref. 13 uses the law of mass action[39], or, equivalently, the Saha equation[40] to obtain the distribution of composite particles. This work shows that an equilibrium is established in the space-time evolution of a collision between two heavy ions. Reaction rates for various processes were calculated and found to be fast enough to establish chemical and thermal equilibrium. The concept of a freeze-out volume was introduced. This volume is the largest volume over which an equilibrium is established. Reaction rates fall much faster than expansion rates in the space-time history of the collision and, consequently, equilibrium laws apply to a brief period of expansion. The model assumes that the distribution of composite particles reflect a frozen-in equilibrium state. The form of the law of mass action of chemical equilibrium is very similar to the result of Eq. (62). This similarity is used to obtain an approximate expression for x.

A main result of Ref. 13 is an equation for the number of nuclei with j nucleons, N_j. The division into protons and neutrons is not considered here and spin will be neglected. Then

$$N_j = N_1 \left[\frac{v_0}{V} N_1 \right]^{j-1} e^{E_B(j)/k_B T} Z^*(j) j^{3/2} . \tag{76}$$

The N_1 is the number of nucleons, $E_B(j)$ is the binding energy of a nucleus of j nucleons, and k_B is the Boltzmann's constant. The V is the equilibrium volume, $v_0 = h^3/(2\pi m_p kT)^{3/2}$ with T the temperature and m_p the mass of a nucleon. The $Z^*(j)$ is an internal partition function of the composite (nucleus of j nucleons) and is given by a sum over ground and excited state contributions:

$$Z^*(j) = \sum_{E_n(j)} e^{-E_n(j)/k_B T} . \tag{77}$$

The energies $E_n(j)$ are measured from the ground-state energy. The effects of $Z^*(j)$ will first be neglected. Comparing Eq. (76) with Eq. (62) in the limit $N_1 \sim A$, the x is $\sim V/v_0$. This result can be improved upon by noting that the binding energy $E_B(j)$ depends on j. In fact, taking for $E_B(j)$ a form

$$E_B(j) = a_B(j-1) \tag{78}$$

gives

$$x = \frac{V}{v_0} e^{-a_B/k_B T} . \tag{79}$$

The backshifted form of Eq. (78) has the following properties. First, $E_B(j)$ is backshifted so that $E_B(1)=0$; the unit elements have no binding energy since they are not composites. The binding energy per particle,

$$E_B(j)/j = a_B[1-(1/j)] ,$$

is less for small clusters than for large clusters: $E_B(2)/2 = a_B/2$, $E_B(3)/3 = 2a_B/3, \ldots,$ $E_B(j \gg 1)/j \rightarrow a_B$. The form of Eq. (78) neglects surface effects, $j^{2/3}$ dependence, Coulomb terms (for charged objects), symmetry energy terms (for two component systems), and shell effects. A discussion of nuclear binding energies can be found in Ref. 41. Neglect of these effects represents a limitation of the model when applied to nuclear collisions.

A comment will be made concerning the evaporation limit. For low x, $x \ll 1$, the $Y_A(k,x)$ is given by Eq. (31). For $k=1$ and $A \gg 1$, $Y_A(1, x \ll 1) = x$. The exponential part of x in Eq. (79) is $\exp(-a_B/kT)$, and this factor acts as a barrier against evaporation. The separation energy or work function W for a particle is also $a_B = W$ for Eq. (78) and is an example of Koopman's theorem. Thus, as x varies from $x \ll 1$ to $x \gg A$, the work function barrier against evaporation evolves into a Maxwell-Boltzmann binding energy enhancement factor. Even the volume part V/v_0 is correct in the evaporation limit. The

$$Y_A(1, x \ll 1) = \frac{V}{v_0} e^{-W/kT} \tag{80}$$

can be found in Ref. 42, for evaporation of a particle into a volume V. Thus, a binding energy enhancement factor in the law of mass action becomes a barrier suppression

factor in the evaporation limit of the model.

The contribution of the internal partition function to x is not as easily obtained. Unlike binding energies, very little is known about this quantity. The x of Eq. (79) is modified to read

$$x = \frac{V}{v_0} e^{-a_B/k_B T} f^*(T) , \tag{81}$$

where $f^*(T)$ is the contribution of $Z^*(j)$ to x. The contribution of $Z^*(j)$ to $f^*(T)$ can be obtained in a manner similar to that used to obtain the contribution of the binding energy to x. Again, the monomer of single elements has no internal excitations. Any exponential j dependence in $Z^*(j)$ can be backshifted by $j \rightarrow (j-1)$. The $Z^*(j)$ has contributions from vibrations, rotations, single-particle excitations, many-particle–many-hole excitations, etc. A low-lying high-spin state can make a large contribution because of the spin degeneracy factor $2J+1$ in an internal partition function. Some discussion of $Z^*(j)$ can be found in Refs. 13, 18, 43, and 44.

Not only do bound states contribute to $Z^*(j)$ but also continuum states, resonances, and echoes of them. For example, the partition function for the hydrogen atom diverges when only bound states are considered, but is finite when continuum contributions are included. In fact as $T \rightarrow \infty$, the continuum part exactly cancels the bound state contribution because of Levinson's theorem. For the nuclear case, a study of $Z^*(j)$ was made for $j=2$ using nucleon-nucleon phase shifts.[13] Indeed, echoes (decreasing phase shifts) tend to cancel bound state or "resonant" (increasing phase shifts) contributions to $Z^*(j)$. For heavy systems (large j), Fermi gas calculations of $Z^*(j)$ (Ref. 43) have been given but these calculations give very large values of $Z^*(j)$ as discussed in Ref. 44. Reference 44 proposes an arbitrary cutoff in $Z^*(j)$ which was used in Ref. 17. A possible form for x is

$$x \sim \frac{V}{v_0} \exp\left[-\frac{a_B}{k_B T} - \frac{k_B T}{\epsilon_0} \left[\frac{T_0}{T+T_0} \right] \right] . \tag{82}$$

The ϵ_0 is the nuclear level density parameter and is about 8 MeV from experiment. The T_0 is an arbitrary cutoff temperature. The mass dependence of $(j^{3/2} Z^*(j))$ in Eq. (76) is taken to be j^{-1} so as to generate the simple solution given in this paper. Until a better understanding of internal partition functions is developed, the form of Eq. (82) can only be considered an approximate representation. The model discussed here was introduced to capture some of the essences of the different fragmentation modes rather than the individual details of them.

III. SUMMARY

This paper proposes a model which may be used to study fragmentation phenomena. The model is exactly soluble in all regimes of an evolutionary tuning parameter. As this evolutionary parameter is varied, various modes of fragmentation rise and fall. A whole spectrum of fragmentation schemes from the simplest to the most complex are contained in one simple expression. The spectrum ranges from a totally fused mode, to evaporation-like modes, to scale-invariant power law behavior, to regions of linear growth of small clusters and exponential falloff of large clusters, to total multifragmentation. Properties of the multiplicity distribution of fragments are developed.

The proposed model gives rise to an exact hyperbolic power law behavior in the cluster size distribution function at a particular value of the evolutionary tuning parameter. At this point, the frequency of occurrence of a cluster of a given size becomes scale invariant. Changing the length scale does not change the distribution law. Each row in Young's triangular lattice of partitions has a distribution law of cluster sizes identical to any other row. Cellular rules are given for generating rows on this triangular lattice. Row by row, the law $Y_A(k)=1/k$, for $k=1,2,\ldots,A$ evolves as A is increased and the end point on the hyperbola at $k=A$ is moved one step over as $A \rightarrow A+1$. A rotation of Ferrer's block diagrams of partitions was proposed and a collision of two systems was viewed as a tumbling of blocks off two columns which represent the target and projectile partitions.

The cumulative mass distribution of the cluster size distribution function was found to have a staircase behavior near the self-similar point. The continuous limit of the staircase function is that of a uniform bar. This uniform bar may be hammered in various ways. One way was to vary the evolutionary tuning parameter which produced various homogeneous distributions. Another, more exotic way, which was presented for its mathematical curiosity rather than its physical realizability, results in Cantor's devil's staircase.

Finally, the solution in the multifragmentation region is compared to results of a model of composite particle formation based on the Saha equation or law of mass action. Properties of the tuning parameter x are partly developed for this specific comparison. The evaporation limit for this choice of x is also discussed and the result contains exponential barrier suppression factors.

ACKNOWLEDGMENTS

The author would like to thank H. Neuberger, M. Stephen, V. Swiatecki, V. Weisskopf, and W. Xia for helpful discussions and D. C. Zheng for very helpful assistance. This work was supported in part by the National Science Foundation under Grant No. 86-01597.

[1] D. Stauffer, *Introduction to Percolation Theory* (Taylor & Francis, Philadelphia, 1985).

[2] G. S. Hawkins, Annu. Rev. Astron. Astrophys. **2**, 149 (1964).

[3] P. Bak, C. Tang, and K. Wiesenfeld, Phys. Rev. Lett. **59**, 381 (1987); Phys. Rev. A **38**, 364 (1988).

[4] L. Kadanoff, S. Nagel, L. Wu, and S. Zhou, Phys. Rev. A **39**, 6524 (1989).

[5] B. Gutenberg and C. F. Richter, Ann. Geophys. **9**, 1 (1956).

[6]M. E. Fisher, Physics (N.Y.) **3**, 255 (1967).
[7]G. Zipf, *Human Behavior and the Principle of Least Effort* (Hafner, New York, 1972).
[8]V. Pareto, *Cours d'Economie Politique* (Publisher, Lausanne, 1987).
[9]A. J. Lotka, J. Wash. Acad. Sci. **16**, 317 (1926).
[10]E. W. Montroll and B. J. West, *Fluctuation Phenomena,* edited by E. W. Montroll and J. L. Lebowitz (North-Holland, Amsterdam, 1976).
[11]B. B. Mandelbrot, *The Fractal Geometry of Nature* (Freeman, San Francisco, 1982).
[12]A. Z. Mekjian, Phys. Rev. Lett. **64**, 2125 (1989).
[13]A. Z. Mekjian, Phys. Rev. C **17**, 1051 (1978).
[14]H. Jaqaman, A. Z. Mekjian, and L. Zamick, Phys. Rev. C **27**, 2782 (1983); **29**, 2067 (1984).
[15]G. Fai and A. Z. Mekjian, Phys. Lett. **169B**, 281 (1987).
[16]A. Goodman, J. Kapusta, and A. Z. Mekjian, Phys. Rev. C **30**, 851 (1984).
[17]A. R. DeAngelis and A. Z. Mekjian, Phys. Rev. C **40**, 105 (1989).
[18]J. Randrup and S. Koonin, Nucl. Phys. **A356**, 223 (1981).
[19]J. Bondorf, R. Donangelo, I. Mishustin, C. Pethick, H. Schultz, and K. Sneppen, Nucl. Phys. **A443**, 321 (1985); J. Bondorf, R. Donangelo, I. Mishustin, and H. Schultz, *ibid.* **A444**, 460 (1985).
[20]D. H. E. Gross, L. Sapathy, M. Ta-Chung, and M. Sapathy, Z. Phys. A **309**, 41 (1982); D. H. E. Gross and X. Zhang, Phys. Lett. **161B**, 47 (1985).
[21]W. A. Friedman and W. G. Lynch, Phys. Rev. C **28**, 950 (1983).
[22]L. Csernai and J. Kapusta, Phys. Rep. **131**, 223 (1986).
[23]G. Bertsch and P. Siemens, Phys. Lett. **126B**, 9 (1983).
[24]S. Levit and P. Bonche, Nucl. Phys. **A437**, 426 (1985).
[25]G. Fai and X. Randrup, Nucl. Phys. **A474**, 173 (1987).
[26]S. Sobotka and L. Moretto, Phys. Rev. C **31**, 668 (1985).
[27]J. Aichelin and J. Hufner, Phys. Lett. **136B**, 15 (1984); J. Aichelin, J. Hufner, and R. Ibara, Phys. Rev. C **30**, 107 (1984).
[28]S. Wolfram, *Theory and Applications of Cellular Automata* (World Science, Singapore, 1986).
[29]M. Abramowitz and I. Stegun, *Handbook of Mathematics Functions,* Natl. Bur. Stand. Appl. Math. Ser. No. 55, (U.S. GPO, Washington, D.C., 1965).
[30]J. Riordan, *An Introduction to Combinatorial Analysis* (Wiley, New York, 1958).
[31]G. H. Hardy, *Ramanujan, Twelve Lectures on Subjects Suggested by His Life and His Work* (Chelsa, New York, 1959).
[32]A. Young, Proc. London Math. Soc. **34**, 361 (1902); **28**, 255 (1927).
[33]J. M. Blatt and V. F. Weisskopf, *Theoretical Nuclear Physics* (Wiley, New York, 1952).
[34]R. Leighton, *Principles of Modern Physics* (McGraw-Hill, New York, 1959).
[35]W. Bauer, D. R. Dean, U. Mosel, and U. Post, Phys. Lett. **150B**, 53 (1985); Nucl. Phys. **A452**, 699 (1986).
[36]X. Campi, J. Phys. A **19**, L917 (1986).
[37]J. Desbois, Nucl. Phys. **A466**, 724 (1987).
[38]C. Cerruti, J. Desbois, R. Boisgard, C. Ngo, J. Natowitz, and J. Nemeth, Nucl. Phys. **A476**, 74 (1988).
[39]P. Morse, *Thermal Physics* (Benjamin/Cummings, Reading, Mass., 1969).
[40]M. N. Saha, Philos. Mag. **40**, 472 (1920); D. D. Clayton, *Principles of Steller Evolution and Nucleosynthesis* (McGraw-Hill, New York, 1968).
[41]W. Myers and V. Swiatecki, Nucl. Phys. **81**, 1 (1966).
[42]E. Fermi, *Thermodynamics* (Dover, New York, 1956).
[43]W. Fowler, C. Engelbrecht, and S. Woosley, Astrophys. J. **226**, 984 (1978).
[44]S. Koonin and J. Randrup, Nucl. Phys. **A474**, 173 (1987).